Inorganic Chemistry

Article

pubs.acs.org/IC

Multichromophoric Bimetallic Ru(II) Terpyridine Complexes Based on Pyrenyl-bis-phenylimidazole Spacer: Synthesis, Photophysics, Spectroelectrochemistry, and TD-DFT Calculations

Srikanta Karmakar, Dinesh Maity, Sourav Mardanya, and Sujoy Baitalik*

Department of Chemistry, Inorganic Chemistry Section, Jadavpur University, Kolkata 700032, India

Supporting Information

ABSTRACT: A symmetrical bridging ligand, 5,11-bis(4-([2,2′:6′,2″-terpyridine]-4′-yl)phenyl)-4,12-dihydropyreno-[4,5-*d*:9,10-*d*′]diimidazole (**tpy-H_2PhImzPy-tpy**), containing terpyridyl coordinating units connected via a pyrenyl-bis-phenylimidazole spacer have been designed to synthesize a new class of light harvesting bimetallic Ru(II) complexes. The electronic properties of this complexes can be fine-tuned by varying tridentate terminal ligands. Full characterization of the compounds has been done with the help of ^{1}H NMR spectroscopy, high-resolution mass spectrometry, and elemental analysis. Geometry optimization of the complexes was also carried out with density functional theory (DFT). Electronic absorption spectra exhibit a number of very intense $\pi-\pi^*$ and n$-\pi^*$ transitions in the UV and moderately intense MLCT and ILCT transitions in the visible region. Interestingly, the present bimetallic complexes exhibit moderately strong luminescence in the range between 657 and 703 nm and lifetimes (long component) between 5.8 and 67.0 ns at room temperature showing the dependence of the emission characteristics upon the type of terminal ligand and solvent. Detailed temperature-dependent emission measurements showed that an overall enhancement of photoluminescence intensity and lifetime occur in all three cases upon lowering of temperature. The redox behavior of the compounds is characterized by a single reversible anodic wave corresponding to two closely spaced one-electron processes. The appearance of intervalence charge transfer transition (IVCT) bands in the NIR region on electrochemical generation of $Ru^{II}Ru^{II}/Ru^{II}Ru^{III}$ species indicates the presence of substantial electronic communication among the two ruthenium centers in the bimetallic complexes. DFT and TDDFT calculations were also done for better understanding of the absorption and emission spectral characteristics of the complexes.

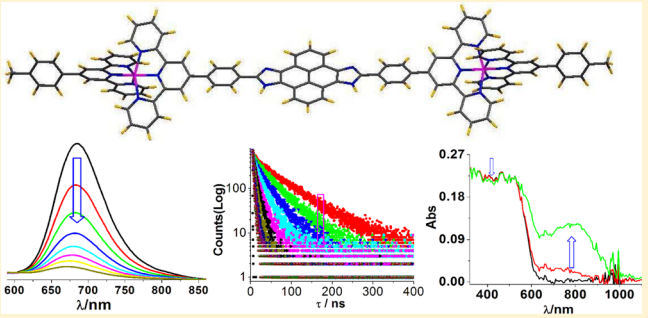

INTRODUCTION

Due to huge scarcity of conventional energy, the conversion of light energy to either electrical or chemical energy by means of artificial photosynthesis is now-a-days a big challenge to the whole scientific community.[1−5] During the past few years increasing attention has been devoted to multichromophoric systems capable of operating as light-harvesting antennae.[6−9] If one of these chromophores is also a good ligand for metal ions, interesting properties can arise in a supramolecular system by changing the bound metal ion. Transition metal polypyridine complexes and in particular Ru(II) complexes exhibiting long-lived luminescent excited state are extensively studied for their potential application in diverse areas such as light harvesting, luminescence sensing, and DNA probes, etc.[10,11] Among the polypyridines, 2,2′:6′,2″-terpyridine (tpy) provides an ideal building block for the development of molecular systems around photoactive metal centers.[12,13] The main advantages of the tpy over bpy are its facile functionalization, the ability to construct linear rod-like structures, and the achiral nature of the resultant complexes.[12,14] A major drawback, however, is the very short (τ < 1 ns) triplet state lifetime that was observed with bis-terpyridine Ru(II) complex at room temperature.[15] This short triplet lifetime, which precludes luminescence in fluid solution, is caused by coupling between the lowest-energy emitting ^{3}MLCT state and a higher-energy nonemitting ^{3}MC state.[12,16] Improvement of luminescence characteristics of these complexes can be done by electronic and structural control of the coordinating ligands such as incorporating electron-withdrawing and electron-donating substituents, enhancing delocalization through the organic moiety, changing the pyridine rings by suitable heterocycles or by using cyclometalating ligands.[17−25] Low-lying ligand-localized excited states with slow decay kinetics are of immense interest because they can prolong the lifetimes of Ru(II) compounds through equilibration with MLCT states or by acting as distinct states.[26] In this context, photophysical properties of a number of Ru(II)-bipyridine complexes with a bridging or pendant pyrene unit studied by several research groups showed that the lifetimes of these complexes are mainly controlled by the excited-state equilibrium between the ^{3}MLCT and ^{3}LC states.[27−34] As compared to Ru-bpy, Ru-tpy complexes containing pyrene unit(s) have

Received: July 19, 2014
Published: November 6, 2014

Chart 1

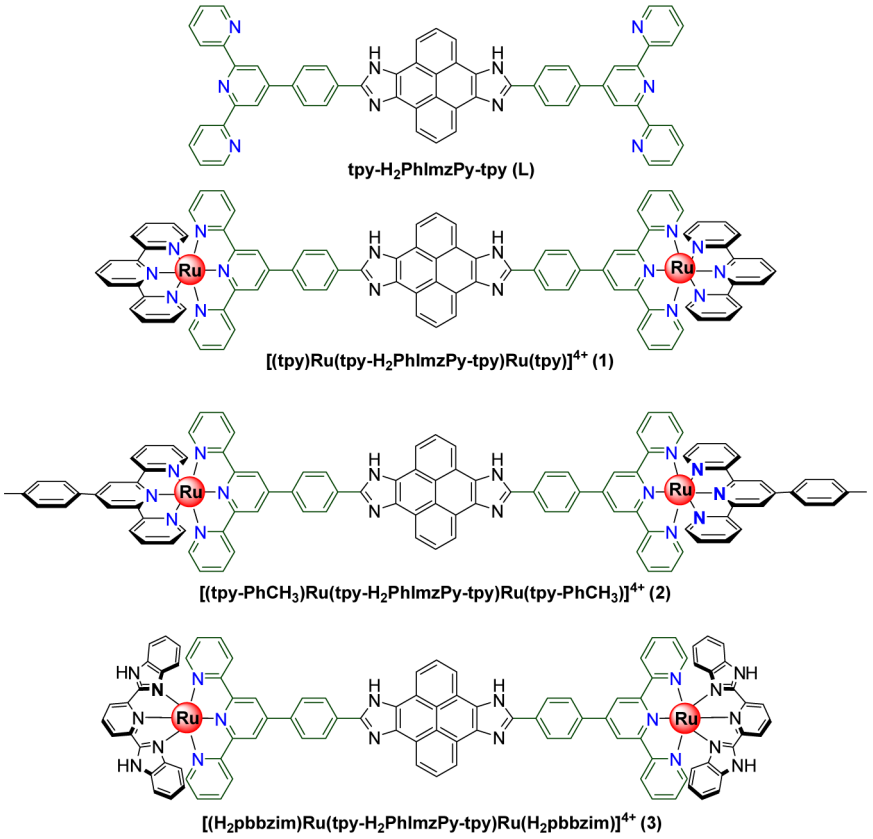

not been well-investigated, in part because of their inferior photophysical properties relative to their bipyridine analogues.[24d,35−37] We are reporting here a new family of bis-terpyridine bridging ligand containing pyrenyl-bis-phenylimidazole spacer. To design the bridging ligand (**tpy-H_2PhImzPy-tpy**), pyrene-4,5,9,10-tetraone core has been utilized because of its geometry and interesting photophysical and electrochemical properties. Herein we report on the synthesis, characterization, photophysical properties, and spectroelectrochemical behaviors of a new family of bimetallic Ru(II) complexes derived from the said bis-terpyridine bridge. For modulation of the physicochemical properties of the complexes, different terminal ligands have been used as shown in Chart 1. In a previous communication, we reported the synthesis and physicochemical behaviors of luminescent monometallic ruthenium(II) and osmium(II) complexes derived from pyrene-phenylimidazole-terpyridine conjugate (tpy-HImzPy), obtained by condensation of pyrene-4,5-dione and tpy-PhCHO.[37] We are now interested to see the influence of the bridging and auxiliary ligands on the photophysical properties of the newly synthesized bimetallic complexes and also to compare with those of the previously reported monometallic compounds. In this study, it is expected that the ^{3}MLCT state should be much more delocalized by the pyrene moiety which can be favorable for the enhancement of their excited-state lifetimes at room temperature. Apart from excited-state delocalization, it is also expected that the introduction of the pyrene moiety may lead to an equilibrium between the excited ^{3}MLCT state and a triplet ($^3\pi-\pi^*$) state mainly situated in the pyrene unit which in turn can also give rise to longer excited-state lifetime. Temperature-dependent photoluminescence study and DFT and TDDFT calculations performed on the complexes provide deeper insight for the understanding of their excited-state behaviors. It will be seen that the appearance of intervalence charge transfer transition (IVCT) bands in the NIR region due to electrochemical generation of mixed-valence $Ru^{II}Ru^{II}/Ru^{II}Ru^{III}$ species will provide useful information regarding the extent of electronic coupling between the ruthenium centers through the bridge.[38−41]

EXPERIMENTAL SECTION

Materials. We procured the raw materials from Sigma-Aldrich Chemicals Co. and used them without further purification. Pyrene-4,5,9,10-tetraone was prepared following the literature procedure.[42] 4′-(*p*-Formylphenyl)-2,2′:6′,2″-terpyridine (tpy-PhCHO), [(tpy)$RuCl_3$], [(tpy-$PhCH_3$)$RuCl_3$], and [(H_2pbbzim)$RuCl_3$] were prepared by literature methods.[24,43]

Synthesis of the Bridging Ligand. 5,11-Bis(4-([2,2′:6′,2″-terpyridine]-4′-yl)phenyl)-4,12-dihydropyreno[4,5-*d*:9,10-*d*′]-diimidazole (tpy-H_2PhImzPy-tpy). To a suspension of pyrene-4,5,9,10-tetraone (0.13 g, 0.5 mmol) and NH_4OAc (1.6 g, 20 mmol) in CH_3COOH (15 mL) was added 0.42 g of tpy-PhCHO (1.25 mmol) slowly with continuous stirring. After complete addition of tpy-PhCHO, the content was refluxed for 3 h. Upon cooling to room temperature, a solid yellow mass was deposited. The compound was then filtered, washed several times with H_2O and methanol, and dried. Yield 0.34 g (75%). Anal. Calcd for tpy-H_2PhImzPy-tpy, $C_{60}H_{36}N_{10}$: C, 80.34; H, 4.05; N, 15.61. Found: C, 80.30; H, 4.09; N, 15.65. ^{1}H NMR (300 MHz, DMSO-d_6): δ 13.94 (s, 2H, NH imidazole), 8.87 (d, 4H, J = 7.8 Hz, H9), 8.78 (s, 4H, H3′), 8.69 (d, 4H, J = 8.0 Hz, H6), 8.55 (d, 4H, J = 7.5 Hz, H3), 8.35 (t, 6H, J = 7.7 Hz, 4H8 + 2H10), 8.20 (d, 4H, J = 8.4 Hz, H7), 8.08 (t, 4H, J = 7.6 Hz, H4), 7.58 (dd, 4H, J = 5.5,4.3 Hz, H5).

Synthesis of [(tpy)Ru(tpy-H_2PhImzPy-tpy)Ru(tpy)](ClO_4)$_4$·2H_2O (1). A mixture of tpy-H_2PhImzPy-tpy (0.14 g, 0.15 mmol) and [(tpy)Ru]Cl_3 (0.13 g, 0.30 mmol) in 20 mL of CH_2OH-CH_2OH

dx.doi.org/10.1021/ic501741r | *Inorg. Chem.* 2014, 53, 12036−12049

Table 1. ^{1}H NMR (500 MHz) Spectral Data of tpy-H_2PhImzPy-tpy and Complexes 1−3 in DMSO-d_6[a]

proton	tpy-H_2PhImzPy-tpy	1	2	3
H(3)	8.55, d(7.5), 4H	7.46, d(5.5), 4H	7.60, d(6.6), 4H	7.66, d(7.5), 4H
H(4)	8.08, t(7.6) 4H	8.03, t(7.5), 4H	8.15−8.07, m, 4H	7.98, dd(6.5, 8.0), 4H
H(5)	7.58, dd(5.5, 4.3), 4H	7.31−7.27, m, 4H	7.35−7.29, m, 4H	7.30−7.25, m, 4H
H(6)	8.69, d(8.0), 4H	8.84, d(8.5), 4H	9.19−9.12, m, 4H	9.08, d(7.5), 4H
H(7)	8.20, d(8.4), 4H	8.73, d(7.5), 4H	8.80, nr, 4H	8.86−8.81, m, 4H
H(8)	8.35, t(7.7), 4H	8.80, d(7.5), 4H	8.80, nr, 4H	8.91, d(8.0), 4H
H(9)	8.87, d (7.8) 4H	8.92, d(7.5), 4H	9.00, d(7.8), 4H	9.00, d(7.5), 4H
H(10)	8.35, t(7.7), 2H	8.30, dd(8.0, nr), 2H	8.39, dd(8.7, nr), 2H	8.39, dd(8.0, nr), 2H
H(11)		7.58, d(6.0), 4H		
H(12)		8.09, t(7.5), 4H		
H(13)		7.31−7.27, m, 4H		
H(14)		9.16, d(8.0), 4H		
H(15)		9.10, d(8.0), 4H		
H(16)		8.55, dd(8.0, nr), 2H		
H(17)				8.65, dd(8.0, nr), 2H
H(18)				8.86−8.81, m, 4H
H(19)				7.51, d(5.5), 4H
H(20)				7.30−7.25, m, 4H
H(21)				7.05, dd(8.5, 7.5), 4H
H(22)				6.11, d(8.5), 4H
H(3′)	8.78, s, 4H	9.60, s, 4H	9.64, s, 4H	9.71, s, 4H
H(3″)			7.60, d(6.6), 4H	
H(3‴)			9.49, s, 4H	
H(4′)			8.15−8.07, m, 4H	
H(5′)			7.35−7.29, m, 4H	
H(6′)			9.19−9.12, m, 4H	
H(7′)			7.60, d(6.6), 4H	
H(8′)			8.39, dd(8.7), 4H	

[a]The atom labeling scheme is shown in Figure 1. Order of data follows, respectively: chemical shift (ppm), multiplicity, J (Hz), number of protons. Multiplicity abbreviations: s = singlet, d = doublet, dd = doublet of doublet, t = triplet, m = multiplet (overlap), nr = not clearly resolved (overlap or shoulder).

was refluxed for 18 h in inert atmosphere, and then cooled and poured into a saturated aqueous solution of $NaClO_4$. The deposited mass was collected by filtration. The crude product was purified by neutral alumina column chromatography using MeCN as the eluent. Further purification of the compound was done by recrystallizing it from MeCN−MeOH (1:1 v/v) mixture under weakly acidic conditions. The resulting compound appeared as red powder. Yield: 0.19 g, 64%. Anal. Calcd for [(tpy)Ru(tpy-H_2PhImzPy-tpy)Ru (tpy)]$(ClO_4)_4$·$2H_2O$, $C_{90}H_{62}N_{16}Cl_4O_{18}Ru_2$: C, 54.06; H, 3.12; N, 11.21. Found: C, 53.98; H, 3.18; N, 11.24. ^{1}H NMR (500 MHz, DMSO-d_6): δ 14.45 (s, 2H, NH imidazole), 9.60 (s, 4H, H3′), 9.16 (d, 4H, J = 8.0 Hz, H14), 9.10 (d, 4H, J = 8.0 Hz, H15), 8.92 (d, 4H, J = 7.5 Hz, H9), 8.84 (d, 4H, J = 8.5 Hz, H6), 8.80(d, 4H, J = 7.5 Hz, H8), 8.73 (d, 4H, J = 7.5 Hz, H7), 8.55 (dd, 2H, J = 8.0, nr Hz, H16), 8.30 (dd, 2H, J = 8.0, nr Hz, H10), 8.09 (t, 4H, J = 7.5 Hz, H12), 8.03 (t, 4H, J = 7.5 Hz, H4), 7.58 (d, 4H, J = 6.0 Hz, H11), 7.46 (d, 4H, J = 5.5 Hz, H3), 7.31−7.27 (m, 8H, 4H5 + 4H13). ESI-MS (positive, MeCN) m/z = 313.51 (40%) [(tpy)Ru(tpy-H_3PhImzPy-tpy)Ru(tpy)]$^{5+}$, 391.88(100%) [(tpy)Ru(tpy-H_2PhImzPy-tpy)Ru (tpy)]$^{4+}$, 522.16 (3%) [(tpy)Ru(tpy-HPhImzPy-tpy)Ru(tpy)]$^{3+}$.

Synthesis of [(tpy-PhCH$_3$)Ru(tpy-H_2PhImzPy-tpy)Ru(tpy-PhCH$_3$)](ClO$_4$)$_4$·H_2O (2). Complex **2** was prepared in the same way as **1** substituting [(tpy-PhCH$_3$)Ru]Cl_3 (0.16 g, 0.30 mmol) for [(tpy)Ru]Cl_3, giving red powdered compound. Yield: 0.21 g, 66%. Anal. Calcd for [(tpy-PhCH$_3$)Ru(tpy-H_2PhImzPy-tpy)Ru(tpy-PhCH$_3$)]$(ClO_4)_4$·H_2O, $C_{104}H_{72}N_{16}Cl_4O_{17}Ru_2$: C, 57.78; H, 3.36; N, 10.37. Found: C, 57.70; H, 3.43; N, 10.32. ^{1}H NMR (500 MHz, DMSO-d_6): δ14.61 (s, 2H, NH imidazole), 9.64 (s, 4H, H3′), 9.49 (s, 4H, H3‴), 9.19−9.12 (m, 8H, 4H6 + 4H6′), 9.00 (d, 4H, J = 7.8 Hz, H9), 8.80 (nr, 8H, 4H7 + 4H8), 8.39 (dd 6H, J = 8.7,nr Hz, 4H8′ + 2H10), 8.15−8.07 (m, 8H, 4H4 + 4H4′), 7.60 (d, 12H, J = 6.6 Hz, 4H3 + 4H3″ + 4H7′), 7.35−7.29 (m, 8H, 4H5 + 4H5′), 2.53 (s, 6H, CH_3). ESI-MS (positive, MeCN) m/z = 349.65 (28%) [(tpy-PhCH$_3$)Ru(tpy-H_3PhImzPy-tpy)Ru(tpy-PhCH$_3$)]$^{5+}$; 436.57 (100%) [(tpy-PhCH$_3$)Ru(tpy-H_2PhImzPy-tpy)Ru(tpy-PhCH$_3$)]$^{4+}$.

Synthesis of [(H_2pbbzim)Ru(tpy-H_2PhImzPy-tpy)Ru(H_2pbbzim)](ClO$_4$)$_4$·$2H_2O$ (3). The synthetic procedure for the production of **3** was identical to that of **1**, except [(H_2pbbzim)$RuCl_3$] (0.15 g, 0.30 mmol) was used instead of [(tpy)Ru]Cl_3, to give **3** as a reddish black crystalline compound. Yield: 0.20 g, 62%. Anal. Calcd for [(H_2pbbzim)Ru(tpy-H_2PhImzPy-tpy)Ru(H_2pbbzim)]$(ClO_4)_4$·$2H_2O$, $C_{98}H_{66}N_{20}Cl_4O_{18}Ru_2$: C, 54.63; H, 3.09; N, 13.00. Found: C, 54.66; H, 3.11; N, 13.05. ^{1}H NMR (500 MHz, DMSO-d_6): δ 15.12 (s, 6H, NH imidazole), 9.71 (s, 4H, H3′), 9.08 (d, 4H, J = 7.5 Hz, H6), 9.00 (d, 4H, J = 7.5 Hz, H9), 8.91 (d, 4H, J = 8.0 Hz, H8), 8.86−8.81 (m, 8H, 4H7 + 4H18), 8.65 (dd, 2H, J = 8.0,nr Hz, H17), 8.39 (dd, 2H, J = 8.0,nr Hz, H10), 7.98 (dd, 4H, J = 6.5,8.0 Hz, H4), 7.66 (d, 4H, J = 7.5 Hz, H3), 7.51 (d, 4H, J = 5.5 Hz, H19), 7.30−7.25 (m, 8H, 4H5 + 4H20), 7.05 (dd, 4H, J = 8.5,7.5 Hz, H21), 6.11 (d, 4H, J = 8.5 Hz, H22). ESI-MS (positive, MeCN) m/z = 344.62 (100%) [(H_2pbbzim)-Ru(tpy-H_3PhImzPy-tpy)Ru(H_2pbbzim)]$^{5+}$, 430.52(81%) [(H_2pbbzim)Ru(tpy-H_2PhImzPy-tpy)Ru(H_2pbbzim)]$^{4+}$, 573.71(20%) [(Hpbbzim)Ru(tpy-H_2PhImzPy-tpy)Ru(H_2pbbzim)]$^{3+}$.

Caution! *All the perchlorate salts reported here are potentially explosive and should be handled with care.*

Instruments and Methods. The physical measurements, electrochemical measurements, and theoretical calculation methods were provided in the Experimental Section of the Supporting Information.

RESULTS AND DISCUSSION

Synthesis and Characterization. Pyrene-4,5,9,10-tetraone was subjected to condensation with 2.5 equiv of tpy-PhCHO in

dx.doi.org/10.1021/ic501741r | Inorg. Chem. 2014, 53, 12036−12049

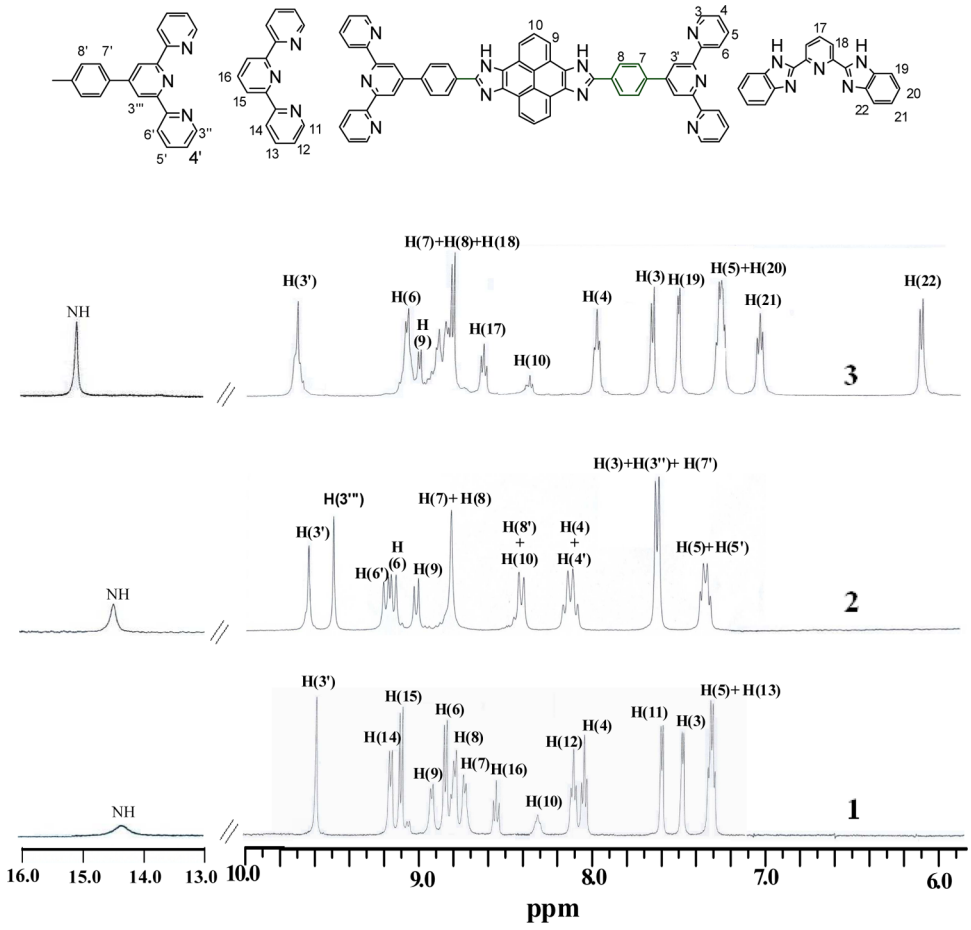

Figure 1. ^{1}H NMR (500 MHz) spectra of **1**−**3** in DMSO-d_6 at room temperature.

a CH_3COOH−NH_4OAc mixture to obtain the bis-terpyridyl bridging ligand, **tpy-H_2PhImzPy-tpy**. The symmetrical bimetallic Ru(II) complexes (**1**−**3**) were synthesized by refluxing tpy-H_2PhImzPy-tpy with appropriate metalloligand in 1:2 ratio in CH_2OH−CH_2OH under inert atmosphere. After purifying by column chromatography, all the complexes are obtained in good yield and characterized with the aid of standard analytical tools and spectroscopic methods.

^{1}H NMR Spectroscopy. The newly synthesized bridging ligand as well as the bimetallic Ru(II) complexes (**1**−**3**) were characterized by recording their ^{1}H NMR, {^{1}H−^{1}H} COSY NMR spectra in DMSO-d_6 solution. Table 1 shows the ^{1}H NMR spectroscopic data of the complexes in DMSO-d_6. Figure 1 displays the ^{1}H NMR spectra of the complexes, and all the signals can be tentatively assigned with the help of COSY NMR studies (Figures S1−S2, Supporting Information). ^{1}H NMR spectral patterns of **1**−**3** reflect the symmetrical environment of two [Ru(tpy/tpy-$PhCH_3$/H_2pbbzim)$_2$] units around the central pyrenyl-phenyl-imidazole spacer. One noteworthy effect on complexation of Ru(II) centers to the free terpyridine sites of the bridge is the downfield shift of protons H3′, H6, H7, H8, and H9 caused by the electron-withdrawing effect of the chelated metal. Moreover, the chemical shifts of the above protons systematically move to the downfield region on going from **1** to **2** and finally to **3**. On the other hand, a significant upfield shift of the bridged H3 proton of the terpyridine moiety occurs (from 8.55 ppm for the free ligand to 7.46−7.66 ppm for the complexes) mainly due to anisotropic ring current effect of an adjacent pyridine and/or phenyl group of the terminal ligand.

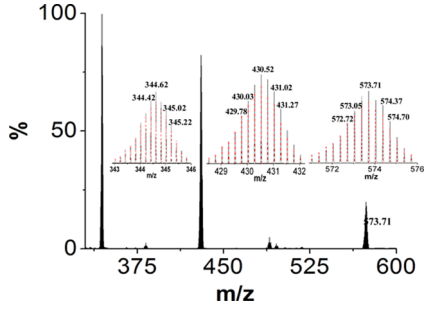

Figure 2. ESI-MS (positive) for the complex cations [(H_2pbbzim)-Ru(tpy-H_3PhImzPy-tpy)Ru(H_2pbbzim)]$^{5+}$ (m/z = 344.62), [(H_2pbbzim)Ru(tpy-H_2PhImzPy-tpy)Ru(H_2pbbzim)]$^{4+}$ (m/z = 430.52), and [(Hpbbzim)Ru(tpy-H_2PhImzPy-tpy)Ru(H_2pbbzim)]$^{3+}$ (m/z = 573.71) in MeCN showing the observed and isotopic distribution patterns. Black solid curves show the experimental values whereas the red dotted vertical lines represent the simulated patterns.

ESI Mass Spectrometry. ESI mass spectrum of **3** along with the assignment of different peak is shown in Figure 2, while those remaining two complexes (**1** and **2**) are presented in Figures S3 and S4 (Supporting Information). It is observed that the bimetallic compounds gave beautiful ESI mass spectra and many of the fragmented ions observed correspond to the species of different oxidation states keeping the bimetallic core intact. Thus, assignments of the various peaks became simplified.

DFT Calculated Structures of Complexes 1−3. DFT optimized structures of **1**−**3** in DMSO (Figure 3) and their structural parameters (Tables S1 and S2, Supporting Information)

dx.doi.org/10.1021/ic501741r | Inorg. Chem. 2014, 53, 12036−12049

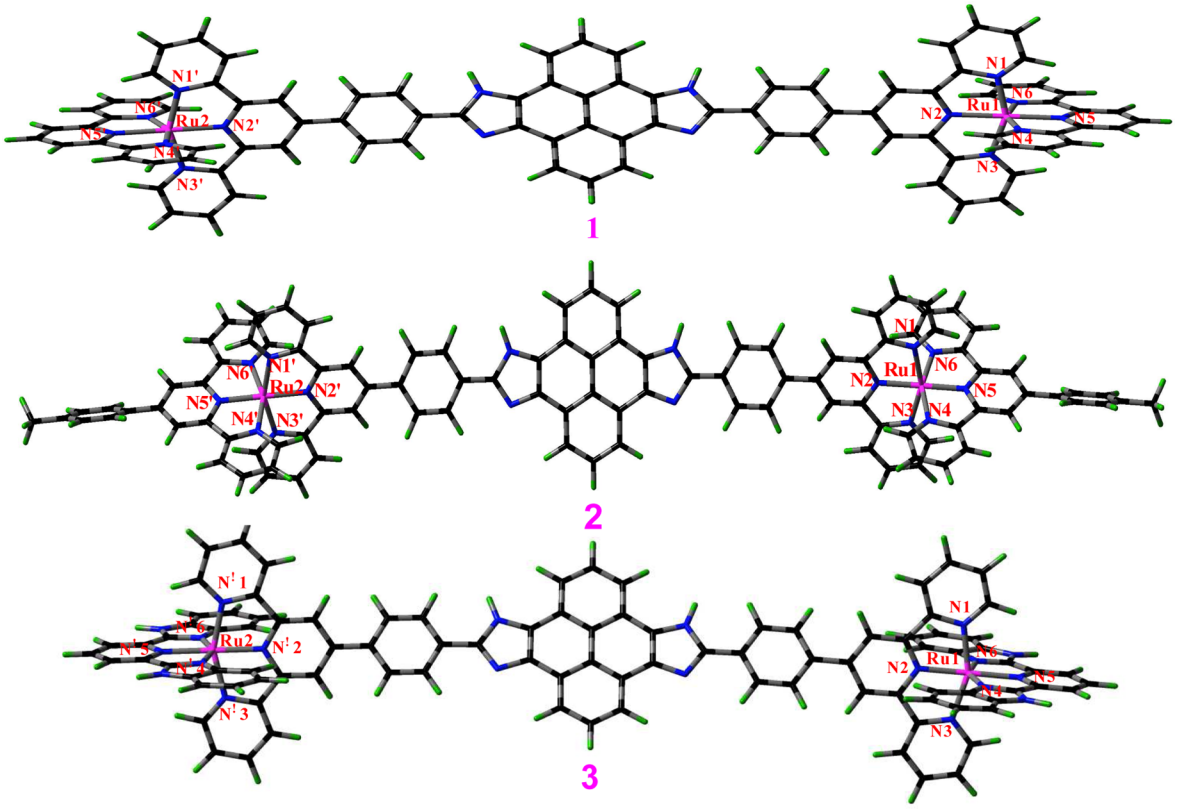

Figure 3. Optimized geometries and labeling schemes of $[(tpy)Ru(tpy\text{-}H_2PhImzPy\text{-}tpy)Ru(tpy)]^{4+}$ (**1**), $[(tpy\text{-}PhCH_3)Ru(tpy\text{-}H_2PhImzPy\text{-}tpy)Ru(tpy\text{-}PhCH_3)]^{4+}$ (**2**), and $[(H_2pbbzim)Ru(tpy\text{-}H_2PhImzPy\text{-}tpy)Ru(H_2pbbzim)]^{4+}$ (**3**) in DMSO.

Table 2. Electrochemical Data[a] for 1−3 in MeCN

	oxidation[b] $E_{1/2}$(ox)/V	ΔE_p/ mV	reduction[c] $E_{1/2}$(red)/V
1	1.43	80	−1.09, −1.48, −1.89
2	1.39	80	−1.19, −1.46, −1.87
3	1.19	60	−1.43, −1.95
$[Ru(tpy)_2]^{2+}$[d]	1.30		−1.29, −1.54
$[Ru(tpy\text{-}PhCH_3)_2]^{2+}$[e]	1.25		−1.24, −1.46
$[Ru(H_2pbbzim)_2]^{2+}$[f]	0.76		−1.40, −1.70

[a]All the potentials are referenced against Ag/AgCl electrode with $E_{1/2}$ = 0.36 V for Fc/Fc^+ couple. [b]Reversible electron transfer process with a Pt working electrode. [c]$E_{1/2}$ values obtained from square wave voltammetric (SWV) using glassy carbon electrode. [d]Data from ref 12a. [e]Data from ref 12a. [f]Data from ref 44a.

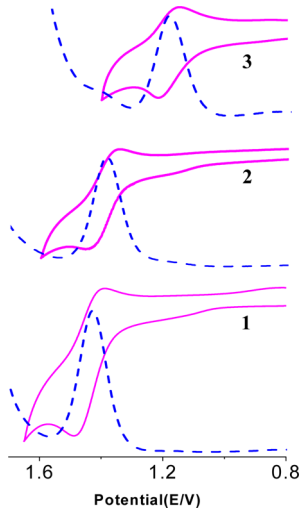

Figure 4. Cyclic (solid line) and square wave voltammograms (dotted line) of complexes **1**−**3** in MeCN at room temperature showing the oxidation of the complexes.

indicate distorted octahedral structure around both Ru(II) centers. The length of the Ru−N bonds varying between 2.000 and 2.122 Å shows similarity with those of related compounds.[17−25] Central Ru−N bonds are shorter than that of the outer Ru−N lengths as expected. It is to be noted that the phenyl rings of **tpy-H$_2$PhImzPy-tpy** in the complexes are rotated to the extent of 34° with respect to the central pyridine of the terpyridine moiety. Moreover, a small twist exists between pyrenyl-imidazole spacer and the phenyl moiety, and the values are in the range 3.03−3.88°. It is of interest to note that nonbonded Ru−Ru distance varying between 30.078 and 30.105 Å is quite large in all the complexes and almost independent of the nature of the terminal ligand as expected.

Redox Properties. The redox behaviors of **1**−**3** in MeCN have been examined through CV and SWV, and the results are summarized in Table 2 and Figure 4. All the compounds display only one reversible oxidation couple corresponding to two simultaneous Ru^{II}/Ru^{III} oxidations at the same potential and several reduction peaks (SWV) due to the reductions of coordinated ligands (Table 2).[44] As can be seen, the incorporation of a $PhCH_3$ moiety to the 4′-position of the tpy decreases the oxidation and reduction potential by approximately 40 and 100 mV, respectively, in **2** compared to **1**. Increasing conjugation on the tpy terminal ligand may be the reason for the decrease of potential in **2**.[12,18] Incorporation of pyridyl-bisbenzimidazole (H_2pbbzim) terminal ligand in **3**, on

dx.doi.org/10.1021/ic501741r | Inorg. Chem. 2014, 53, 12036−12049

Table 3. Spectroscopic and Photophysical Data of tpy-H_2PhImzPy-tpy and 1−3 in DMSO with Their Theoretical Values

	experimental								theoretical	
		luminescence								
		at 298 K[a]				at 77 K[b]				
compd	abs λ_{max}/nm (ε/M^{-1} cm^{-1})	λ_{max}/nm	τ/ns	$\Phi/10^{-3}$	$k_r/10^5$ s^{-1}	$k_{nr}/10^7$ s^{-1}	λ_{max}/nm	Φ	abs λ_{max}/nm (ε/M^{-1} cm^{-1})	luminescence λ_{max}/nm
L	410 (28 600), 387(sh) (21 400) 348 (36 900), 287 (47 000)	528	4.5	301	688	15.3				
1	497 (67 700), 422(sh) (36 000) 357 (sh) (65 700), 334(sh) (99 500) 314 (119 800), 285 (89 100)	664	3.0, 7.0	0.12	0.4, 0.2	33, 14	643	0.24	516 (65 400), 455 (50 000), 396 (59 400), 339 (88 700) 302 (169 100)	627
2	504 (62 400),420(sh) (27 700)360 (sh) (53 200), 334(sh)(94 200) , 317 (108 000), 289 (98 500)	670	3.0, 8.1	0.38	1.3, 0.5	33, 12	647	0.27	520 (83 000), 412 (49 400) 339 (131 400), 306 (185 800)	635
3	610(br) (10 700), 519 (49 400) 416 (sh) (42 800), 350 (101 200) 325 (109 300), 290 (80 400)	703	16.0, 67.0	1.70	1.0, 0.2	6, 1.5	675	0.35	531 (60 400) 441 (56 100), 345 (148 200), 307 (164 600)	645
$[Ru(tpy)_2]^{2+c}$	474 (10 400)	629	0.25	≤0.05	0.04	90.9	598			
$[Ru(tpy\text{-}PhCH_3)_2]^{2+d}$	490 (28 000)	640	<5.0	≤0.03			628, 681 (sh)			
$[Ru(H_2pbbzim)_2]^{2+e}$	475 (17 400)									

[a] In DMSO. [b] MeOH−EtOH (1:4) glass. [c] Data from ref 12a. [d] Data from ref 12a. [e] Data from ref 44a.

the other hand, results in a substantial decrease (~200 mV) in the Ru^{II}/Ru^{III} potential compared with both **1** and **2**. The substantial cathodic shift of Ru-based oxidation in **3** is probably due to stronger electron-donating capability of H_2pbbzim compared with tpy-type ligands.

Absorption Spectra. The electronic absorption spectra of **1**−**3** were recorded in both MeCN and DMSO, and the accumulated data were presented in Table 3 and Table S3 (Supporting Information). Figure 5 and Figure S5 (Supporting Information) display the UV−vis absorption spectra of **1**−**3** and **tpy-H_2PhImzPy-tpy**. Due to solubility limitation, the spectrum of **tpy-H_2PhImzPy-tpy** was recorded only in DMSO. As for most other terpyridyl-bridged complexes of Ru(II), the UV−vis absorption spectra of **1**−**3** mainly consist of MLCT and ILCT transitions in the visible and ligand-based $\pi \rightarrow \pi^*$ and $n \rightarrow \pi^*$ transitions in the UV region.[12,17−25] The intense band in the range of 480−520 nm can be attributed to $Ru^{II}(d\pi) \rightarrow$ tpy MLCT transition on the basis of the previous studies of the related bis-terpyridine complexes of Ru(II).[12] It will be seen later by TD-DFT calculation that a substantial amount of intraligand-charge transfer (ILCT) character from pyrenyl-imidazole moiety to the tpy unit of the bridge tpy-H_2PhImzPy-tpy contributes to this band. Absorption spectra of the complexes also contain a broad band in low-energy region (lying between 570 and 610 nm, depending upon the terminal ligand and solvent). This band probably arises from $^1[Ru^{II}(d\pi)^6] \rightarrow {}^3[Ru^{II}(d\pi)^5$tpy-$H_2$PhImzPy-tpy$(\pi^*)^1]$ transitions which are allowed due to spin−orbit coupling which has the effect of mixing excited singlet and triplet states.[16a,45] The MLCT bands are assumed to contain contributions arising from electron injection into both bridging and terminal ligands. It is important to mention that the red-shift of the lowest energy spin-allowed band occurs with the concomitant decrease in molar extinction coefficient as we go across from complex **1** to complex **3**. A significant broadening and a bathochromic shift for the ^{1}MLCT band occurs in **3** compared to both **1** and **2** probably because of the asymmetric coordination environment in **3** caused by the coordination of **H_2pbbzim** and tpy site of **tpy-H_2PhImzPy-tpy** bridge. The intensities of the MLCT bands of the present complexes are quite high as expected and comparable to those of reported bichromophoric complexes of this type (Table 3).[12,18]

Figure 5. UV−vis absorption spectra of tpy-H_2PhImzPy-tpy (**L**) and complexes **1**−**3** in DMSO.

Emission Spectra. The photoluminescence behaviors of the compounds were investigated in both fluid solution (MeCN and DMSO) at 298 K and in frozen matrix at 77 K (Figure 6 and Figure S5 Supporting Information), and the relevant parameters are summarized in Table 3 and Table S3 (Supporting Information). On excitation at 410 nm, tpy-H_2PhImzPy-tpy fluoresces strongly (Φ = 0.301) at 528 nm in

dx.doi.org/10.1021/ic501741r | Inorg. Chem. 2014, 53, 12036−12049

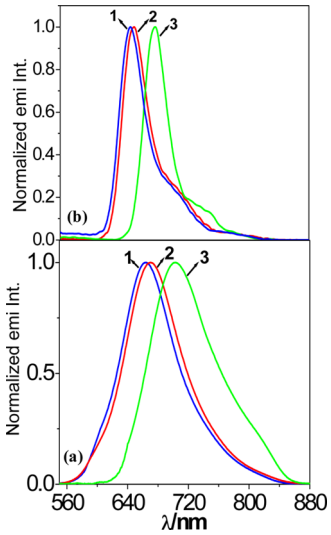

Figure 6. Photoluminescence spectra of complexes **1**−**3** in DMSO at room temperature (a) and in EtOH−MeOH (4:1) glass at 77 K (b).

DMSO having τ value of 4.5 ns (Figure S6, Supporting Information). The excitation wavelength was chosen as 490 nm in each case. It is observed that the emission profiles remain independent of excitation wavelength, and there is also close similarity between excitation spectra and electronic spectra of the complexes. Emission maximum of the compounds lies in the range 657−703 nm depending upon the terminal ligand as well as solvent. Excited-state decay profiles of **1**−**3**, measured by TCSPC, are presented in Figure S7 (Supporting Information). The observed decay profiles can be fitted with a double-exponential function in each case. Fitting of the decay profiles provides a short lifetime component with τ_1 varying between 1.7 and 8.0 ns in MeCN and between 3.0 and 16.0 ns in DMSO. The long component of the complexes, on the other hand, possesses a lifetime (τ_2) in the domain 5.8−24.2 ns in MeCN and 7.0−67.0 ns in DMSO (Figure S7, Supporting Information). The initial short lifetime corresponds to the deactivation of ^{3}MLCT state localized on terpyridine site of tpy-H_2PhImzPy-tpy, whereas subsequent long lifetime may originate as a result of equilibrium with either ^{3}LC or ^{3}ILCT state of pyrene which in turn repopulates the ^{3}MLCT state.[12,16−18] In each case, the emission maximum shifts to longer wavelength as the solvent polarity increases from MeCN to DMSO. The stabilizing influence of a polar solvent is understandable in terms of enhanced charge displacement in the emissive ^{3}MLCT state. With respect to parent $[Ru(tpy)_2]^{2+}$, all three newly synthesized compounds show a bathochromic shift in their emission band (Table 3).[12a] Moreover, at room temperature, the luminescence lifetimes of the bimetallic complexes are appreciably longer than that of either $[Ru(tpy)_2]^{2+}$ (τ = 0.25 ns) or $[Ru(tpy\text{-}PhCH_3)_2]^{2+}$ (τ < 5 ns).[12a] Among three bimetallic complexes, **3** exhibits the highest excited-state lifetime (τ = 24.2 ns in MeCN and τ = 67.0 ns in DMSO). The bathochromic shift of the luminescence band and enhancement of luminescence lifetime of the complexes may be due to substantial stabilization imparted by pyrenyl-phenyl-imidazole spacer, which is connected to the terpyridine in 4′-position, causing an enhanced excitation delocalization. Moreover, it is again interesting to note that the emission quantum yield and lifetimes of these bimetallic complexes are relatively longer than those of the previously reported related mononuclear compounds.[18,19]

The excited-state energies of complexes **1**−**3**, estimated from their emission maxima at 77 K, lie in the range 1.84−1.93 eV which are comparable to those of similar tpy-based ruthenium complexes (Figure 6b).[12,18] Considering these generally quite high excited-state energies and the strongly anodically shifted redox potentials, these complexes appear to be particularly strong excited-state oxidants. Thus, by using eqs 1 and 2) and the CV data (Table 2), the excited-state oxidation potentials of the complexes were calculated to be −0.47, −0.53, and −0.65 V for **1**, **2**, and **3**, respectively, while the excited-state reduction potentials were +0.83, +0.72, and +0.41 V for **1**, **2**, and **3**, respectively.

$$E^*([Ru^{III}Ru^{III}]^{5+}/[Ru^{II}Ru^{II}]^{4+}) = E([Ru^{III}Ru^{III}]^{5+}/[Ru^{II}Ru^{II}]^{4+}) - E_{00} \quad (1)$$

$$E^*([Ru^{II}Ru^{II}(lig)]^{4+}/[Ru^{II}Ru^{II}(lig^{\bullet\bullet-})]^{2+}) = E([Ru^{II}Ru^{II}(lig)]^{4+}/[Ru^{II}Ru^{II}(lig^{\bullet\bullet-})]^{2+}) + E_{00} \quad (2)$$

The possibility of photoinduced electron transfer in **1**−**3** can be evidenced by reductive quenching of the ^{3}MLCT excited state(s) using known reductants such as triethanolamine (TEOA) or ascorbic acid as an electron donor. From the values of the excited-state redox potentials of **1**−**3**, it is evident that the excited complexes should be able to oxidize TEOA to its radical cation $[TEOA]^{\bullet+}$ (E = 0.82 V vs NHE; E = 0.19 V vs Fc/Fc^+).[25] It is observed that quenching of the luminescence occurs in all cases with TEOA, albeit to a different extent (Figure 7). By utilizing the lifetime data in DMSO, the

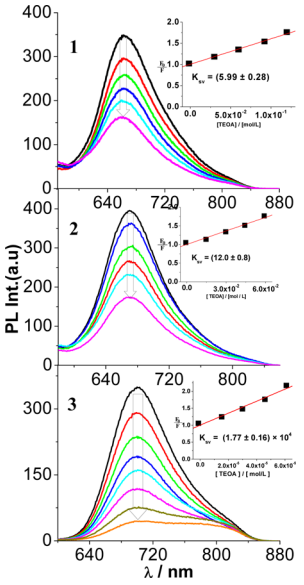

Figure 7. Emission quenching of excited complexes **1**−**3** by TEOA in DMSO at room temperature; the excitation wavelength was 490 nm. The inset of the figure shows the Stern−Volmer plots for the emission quenching by using $F_0/F = 1 + K_{sv} \times [TEOA]$.

bimolecular rate constants k_q ($=K_{sv}/\tau_0$) have been calculated to be 8.55×10^8, 1.48×10^9, and 2.64×10^{11} M^{-1} s^{-1} for **1**, **2**, and **3**, respectively. Ascorbic acid, on the other hand, quenches the luminescence of **3** only (Figure S8, Supporting Information). The present complexes are thus interesting candidates as photosensitizer in applications that require high oxidation power, as for example in water oxidation.

dx.doi.org/10.1021/ic501741r | Inorg. Chem. 2014, 53, 12036−12049

Temperature-Dependent Emission. Both steady state emission spectra and excited-state lifetimes of **1**−**3** were recorded in the temperature range 260−350 K for understanding the decay kinetics of the lowest luminescent ^{3}MLCT state, and the relevant information are presented in Figures 8 and 9 and Table 4. The temperature-dependent luminescence lifetime data of the three complexes were fitted to eq 3.[45,46]

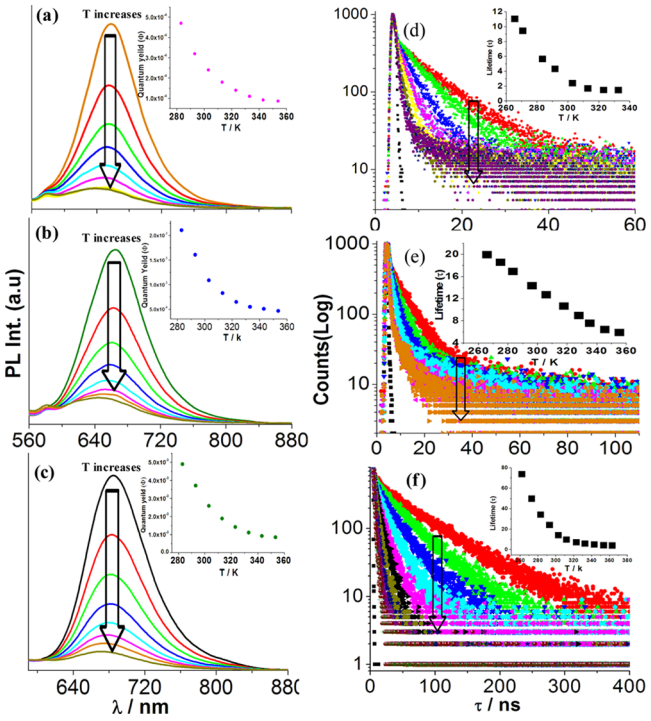

Figure 8. Effect of temperature on steady state emission (a−c) and excited-state decay profiles (d−f) for **1**−**3** in MeCN. The changes of quantum yields and emission lifetimes of the complexes as a function of temperature are shown in the corresponding insets.

$$(\tau(T))^{-1} = (k_1 + k_2 \exp[-\Delta E_2/RT]) / (1 + \exp[-\Delta E_2/RT]) \quad (3)$$

In this equation, k_1 is the temperature-independent rate constant and is the sum of the radiative (k_r) and nonradiative (k_{nr}) decay constants from the ^{3}MLCT state to the ground state at low temperature (77 K). The temperature-dependent rate constant k_2 represents the decay constant for accessing the ligand-field (^{3}MC) state from ^{3}MLCT state, and the activation energy required for this process is represented as ΔE_2. Fitting of the experimental kinetic data to the equation allows calculation of k_1, k_2, and ΔE_2 in the complexes, and values are summarized in Table 4 and Figure 9. The calculated values agree reasonably well with the related Ru(II) compounds.[12] Substantial increase in the energy difference (ΔE_2) between the ^{3}MLCT and ^{3}MC states occurs in **1**−**3** compared with parent $[Ru(tpy)_2]^{2+}$ (ΔE_2 = 1500 cm^{-1}) and $[Ru(tpy\text{-}PhCH_3)_2]^{2+}$ (ΔE_2 = 1800 cm^{-1}), and the increase in ΔE_2 is probably due to extensive delocalization of the bridging ligand induced by the pyrenyl-bis-phenylimidazole spacer.[17−19] The net outcome is the significant enhancement of the room-temperature lifetimes of the present series of Ru(II) complexes without substantial lowering of the ^{3}MLCT energy. Thus, the favorable absorption and emission spectral behaviors along with reasonably long

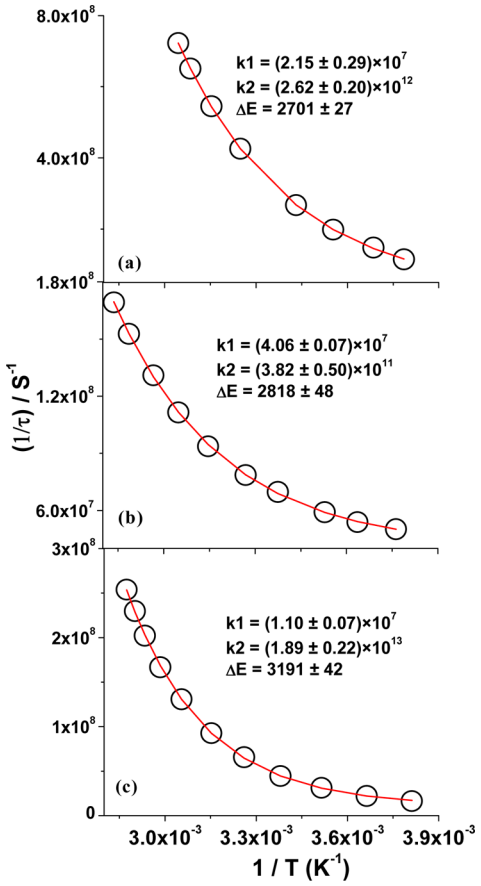

Figure 9. Temperature-dependent lifetime data of **1** (a), **2** (b), and **3** (c) in MeCN with their corresponding nonlinear fits using eq 3 described in the text. Inset shows the values of different parameters.

Table 4. Kinetic Decay Parameters of Complexes 1−3

	$k_{1\ (s^{-1})}$	$k_{2\ (s^{-1})}$	ΔE_2 (cm^{-1})
1	(2.15 ± 0.29) × 10^7	(2.62 ± 0.20) × 10^{12}	2701 ± 27
2	(4.06 ± 0.07) × 10^7	(3.82 ± 0.50) × 10^{11}	2818 ± 48
3	(1.10 ± 0.07) × 10^7	(1.89 ± 0.22) × 10^{13}	3191 ± 42

lifetimes at room temperature highlight the viability of using this bimetallic Ru(II) complexes in light-harvesting applications.

Spectroelectrochemistry. In order to obtain more information about the extent of electron delocalization among the two ruthenium centers in the bimetallic complexes (**1**−**3**), spectroelectrochemical studies were done in MeCN under controlled oxidation in the range between 300 and 2100 nm (Figure 10 and Figures S9−S10 Supporting Information). During electrochemical oxidation for **2**, the ILCT and MLCT transition in the visible (400−500 nm) decreased very little. At the same time, emergence of new absorptions around 600−1100 nm region was evident. Deconvoluting the broad band between 550 and 1100 (inset to Figure 10a,b), we obtained two bands at 566 nm (ν = 17 668 cm^{-1}, ε = 15 285 M^{-1} cm^{-1}) and 792 nm (ν = 12 626 cm^{-1}, ε = 6045 M^{-1} cm^{-1}). The peak at 566 nm can be assigned as tpy-H_2PhImzPy-tpy → Ru^{III} LMCT transition, while the peak at 792 nm can be assigned as IVCT transition. Further electrolysis of the compound ($Ru^{II}Ru^{III}$) gives rise to small decrease of the MLCT bands around 400−500 nm region, substantial decrease of the NIR (600−1100 nm) band, as well as small increase of band around

dx.doi.org/10.1021/ic501741r | Inorg. Chem. 2014, 53, 12036−12049

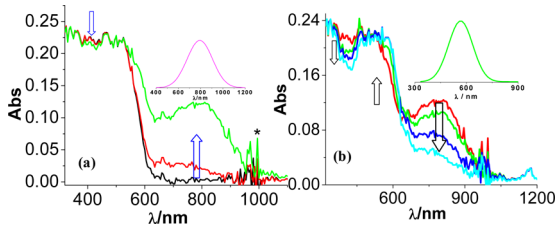

Figure 10. Spectroelectrochemical changes during the oxidation of $[tpy\text{-}PhCH_3)Ru(tpy\text{-}H_2PhImzPy\text{-}tpy)Ru(tpy\text{-}PhCH_3)](ClO_4)_4$ (**2**) in MeCN. The changes involve $Ru^{II}Ru^{II} \rightarrow Ru^{II}Ru^{III}$ (a) and $Ru^{II}Ru^{III} \rightarrow Ru^{III}Ru^{III}$ (b). The IVCT band obtained from spectral deconvolution is shown in inset to part a, and LMCT band obtained from spectral deconvolution is shown in inset to part b. Asterisks denote artifacts due to nonperfect background compensation.

540−580 nm region. Appearance of an isosbestic point is clearly observed in each case (523, 534, and 532 nm for **1**, **2**, and **3**, respectively) during electrochemical oxidation. The fully generated $Ru^{III}Ru^{III}$ complex shows LMCT band between 600 and 800 nm. The spectral patterns of complexes **1** and **3** are basically similar to that of **2** except there is little variation of the λ_{max} and ε values of the IVCT band. The assignment of the band centered around 800 nm as IVCT is confirmed by the decrease of the band when the complexes are fully oxidized. The degree of electronic coupling of the mixed-valence systems can be estimated by analyzing the IVCT band (Table 5).[38−41] The spectral parameters of the IVCT band (low ε value) indicated that the present $Ru^{II}Ru^{III}$ complexes can be categorized as a class II system.[38−41] According to the Hush model,[47] the theoretical value of $\Delta\nu_{1/2}$ for a class II system can be obtained by eq 4.

$$\Delta\nu_{1/2} = (2310E_{op})^{1/2}\ cm^{-1} \quad (4)$$

Table 5 shows that the theoretically predicted values of $\Delta\nu_{1/2}$ are in agreement with the experimentally observed values. The magnitude of the electronic coupling can be calculated with the help of eq 5.[38,47]

$$H_{ab} = [2.06 \times 10^{-2}(\varepsilon_{max}\Delta\nu_{1/2}E_{op})^{1/2}]/r_{ab} \quad (5)$$

where H_{ab} is the magnitude of electronic coupling, and r_{ab} is the effective electron-transfer distance; ε_{max}, $\Delta\nu_{1/2}$, and E_{op} have been explained previously. The effective electron transfer distance between the two ruthenium centers can be obtained from the measurements of the dipole moment change associated with the IVCT processes through electroabsorption (Stark effect) spectroscopy.[38,48] In the absence of these measurements, however, r_{ab} is generally equated with the through-space geometrical distance between the metal centers. In the present case, the values of r_{ab} were estimated by taking the Ru−Ru distance in the DFT optimized structures of the bimetallic complexes **1**−**3** ($r_{ab} \approx 30.066$ Å). Since the geometric distance is likely to be greater than the actual charge transfer distance due to electronic coupling across the bridge, eq 5 provides a lower limit for H_{ab}. Within this approximation, the calculated values of H_{ab} vary only in the range 370−474 cm^{-1} among the compounds studied, despite considerable variation in the electronic properties of the terminal ligands. The value of H_{ab}, although underestimated, also shows that the present compounds belong to class II $Ru^{II}Ru^{III}$ system; for class II $Ru^{II}Ru^{III}$ species, the value of H_{ab} typically varies between 50 and 700 cm^{-1}.[49] It very interesting to note that all the three complexes exhibit moderately strong IVCT band in near IR region despite the fact that the two ruthenium atoms are separated by a large distance, estimated to be around 30 Å. To our knowledge, this is one of the intervalence transitions involving electron transfer over the longest distance.[50]

The parameter Γ also provides a criterion for describing the degree of electronic coupling in mixed-valence systems (eq 6),[39,40] where $0.1 < \Gamma < 0.5$ for weak to moderate

$$\Gamma = 1 - [\Delta\nu_{1/2(expt)}/\Delta\nu_{1/2(theo)}] \quad (6)$$

coupling (localized class II systems), $\Gamma \approx 0.5$ at the class II−III transition, and $\Gamma > 0.5$ for strongly coupled (delocalized class III) systems. In the present $Ru^{II}Ru^{III}$ systems, the values of Γ lying

Table 5. Absorption Spectral Data of the Complexes (1−3) on Spectroelectrochemical Oxidation in MeCN

	E_{op} cm^{-1}	$\Delta\nu_{1/2(exp)}$ cm^{-1}	$\Delta\nu_{1/2(theo)}$	λ_{max}/nm (ε/M^{-1} cm^{-1})	H_{ab}	Γ	λ_{max}/nm (ε/M^{-1} cm^{-1})
1	13 158	6596	5513	760 (3690)	387	0.196	544 (11 400)
2	12 626	6305	5400	792 (6045)	474	0.167	566 (15 285)
3	12 500	6273	5373	800 (3736)	370	0.167	580 (12 478)

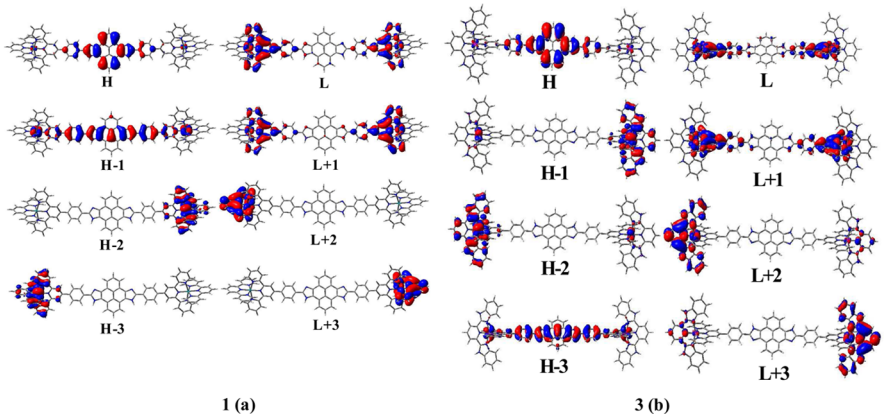

Figure 11. Schematic drawings of the selected frontier molecular orbitals for **1** (a) and **3** (b) in DMSO.

dx.doi.org/10.1021/ic501741r | Inorg. Chem. 2014, 53, 12036−12049

Table 6. Selected UV−Vis Energy Transitions at the TD-DFT/B3LYP Level for1, 2, and 3 in DMSO

excited state	λ_{cal}/nm/ε_{cal}/ M^{-1} cm^{-1}/(eV)	oscillator strength (f)	λ_{expt}/nm/ε_{expt}/ M^{-1} cm^{-1}/(eV)	key transitions	character
1					
S_1	516 (65 400), 2.40	0.89	497 (67 700), 2.49	H → L + 1(94%), H − 1 → L(2%)	ILCT, MLCT
S_{17}	455 (50 000), 2.72	0.60	422(sh) (36 000), 2.93	H − 4 → L + 1(25%), H − 1 → L(37%), H − 7 → L(7%), H − 6 → L + 3(7%), H − 5 → L + 2(8%), H − 3 → L + 4(3%), H − 2 → L + 5(3%)	MLCT, ILCT
S_{33}	396 (59 400), 3.13	0.69	357(sh) (65 700), 3.47	H → L + 9(88%), H → L + 15(3%)	ILCT, π−π*
S_{75}	339 (88 700), 3.65	0.98	334(sh) (99 500), 3.71	H − 1 → L + 8(61%), H → L + 15(22%), H − 4 → L + 9(6%)	ILCT, π−π*, MLCT
S_{129}	302 (169 100), 4.11	0.30	314 (119 800), 3.95	H − 3 → L + 15(26%), H − 3 → L + 16(11%), H − 13 → L (9%), H − 12 → L + 1(4%), H − 3 → L + 8 (6%), H − 3 → L + 12(8%), H − 3 → L + 13(5%), H − 3 → L + 14(4%), H − 2 → L + 15(5%)	MLCT, π−π*,
2					
S_1	520 (83 000), 2.38	1.03	504 (62 400), 2.46	H → L + 1 (94%), H − 1 → L (3%)	ILCT, MLCT
S_{27}	412 (49 400), 3.00	0.76	420(sh) (27 700), 2.95	H − 5 → L + 4 (17%), H − 5 → L + 5(27%), H − 4 → L + 4(26%), H − 4 → L + 5(16%), H − 1 → L(8%)	MLCT
S_{77}	339 (131 400), 3.65	0.97	334(sh) (94 200), 3.71	H − 1 → L + 8(57%), H → L + 15(27%), H − 6 → L + 9(6%), H → L + 9(3%)	ILCT, π−π*, MLCT
S_{134}	306 (185 800), 4.05	0.37	317(108 000), 3.91	H − 15 → L + 2(24%), H − 15 → L + 3(13%), H − 14 → L + 2(13%), H − 14 → L + 3 (24%), H − 17 → L + 2(2%), H − 16 → L + 3(2%), H − 5 → L + 13(4%), H − 4 → L + 12(4%)	π−π*
3					
S_3	531 (60 400), 2.33	0.90	519 (49 400), 2.39	H → L + 1(94%), H − 3 → L(3%)	ILCT, MLCT
S_{21}	441 (56 100), 2.82	0.66	416(sh) (42 800), 2.98	H − 4 → L + 1(11%), H − 3 → L(26%), H − 2 → L + 5(11%), H − 1 → L + 4(11%), H − 6 → L + 3(5%), H − 5 → L + 2(5%), H − 5 → L + 3(2%), H − 2 → L + 6(8%), H − 1 → L + 7(8%)	MLCT, ILCT
S_{69}	345 (148 200), 3.60	0.98	350 (101 200), 3.54	H − 10 → L + 3(43%), H − 9 → L + 2(42%), H − 10 → L + 2(5%), H − 9 → L + 3(5%)	π−π*
S_{132}	307 (164 600), 4.04	0.71	325 (109 300), 3.81	H − 19 → L(40%), H − 18 → L + 1(39%), H − 2 → L + 10 (3%), H − 2 → L + 14(2%), H − 1 → L + 13(5%)	π−π*, MLCT

dx.doi.org/10.1021/ic501741r | Inorg. Chem. 2014, 53, 12036−12049

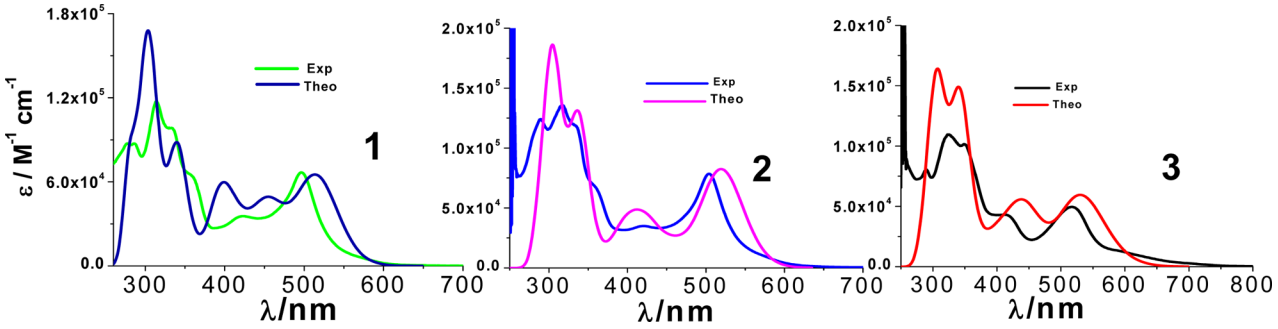

Figure 12. Experimental and calculated absorption spectra of **1**, **2**, and **3** in DMSO at room temperature.

between 0.167 and 0.196 indicate that these are all weakly coupled class II systems.[38−41,51]

COMPUTATIONAL STUDY

Ground-State Electronic Structure. The geometry optimization and electronic structure calculations of the complexes were performed via DFT. The shapes of the frontier orbitals of the complexes are displayed in Figure 11 and Figure S11 (Supporting Information), and their orbital energies and compositions are presented in Table S4 (Supporting Information). The characters and energies of four HOMOs of these complexes resemble each other. It is evident that the electronic population is dominant in the pyrenyl-imidazole part in HOMO and HOMO − 1 for complexes **1** and **2** and in HOMO and HOMO − 3 for **3**, while the contribution of ruthenium is dominant in HOMO − 2 and HOMO − 3 for **1** and **2** and in HOMO − 1 and HOMO − 2 for **3**. The essential character of the LUMOs of each complex is again virtually similar. The electronic population is mainly localized in the bridging tpy ligand in LUMO and LUMO + 1, while the electron density resides on LUMO + 2 and LUMO + 3 in the terminal ligand in all three complexes. It is of interest to note that both HOMOs and LUMOs of **3** are lower in energy relative to those of **1** and **2**, probably because of the larger delocalization throughout the aromatic frame.

Electronic Absorption Spectra. For the proper assignment of the optical spectra, TDDFT computations are carried out with the optimized ground-state structures of **1**−**3**, and the relevant results are delineated in Table 6. Frontier orbitals involved in different transitions are displayed in Figure S12−S18 (Supporting Information). Figure 12 shows the overlay of the calculated and observed absorption spectra of **1**−**3** in DMSO. The computed peak at 516 and 520 nm of **1** and **2** is mainly associated with the S_1 excitation (HOMO → LUMO + 1), while the peak at 531 nm for **3** is associated with the S_3 excitation. This band mainly arises due to a transition from the HOMO orbital containing significant pyrenyl-imidazole character to the LUMO + 1 orbital containing π^*-orbital character on the bridging tpy ligand and thus can be assigned as an intraligand-charge-transfer (ILCT) transition. However, very small amounts of bridged-tpy-based MLCT transitions are also involved (e.g., HOMO − 1 → LUMO for both **1** and **2** and HOMO − 3 → LUMO for **3**) in each case. The next lower energy absorption peak of the complexes in the visible region (412−455 nm) largely originates from the S_{17}, S_{27}, and S_{21} excitation for **1**, **2**, and **3**, respectively. All these excitations have mixed character of MLCT transitions associated with both the bridging and terminal ligands (HOMO → LUMO + 5; HOMO − 4 → LUMO + 1; HOMO − 4 → LUMO + 3). We also note that

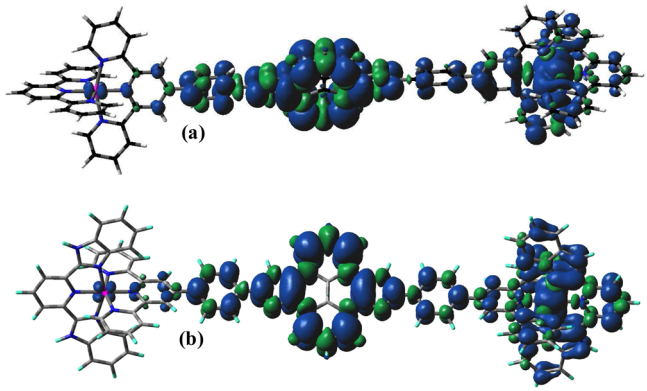

Figure 13. Spin density plots for two-electron-oxidized form of **1** (a) and **3** (b).

there is some contribution due to the electronic transitions within the ligand. In general, three high-energy transitions below 400 nm involve the promotion of electrons from molecular orbitals localized over pyrenyl-imidazole and/or the ruthenium metal and phenyl ring to the π^* system of the bridging as well as terminal tpy ligands. Therefore, electronic transitions that involve these frontier orbitals possess the intrinsic $\pi-\pi^*$ character. The predicted UV−vis absorption spectra match well with the experimental spectra, although the absolute magnitudes of these energies do not overlap closely with those determined experimentally (Figure 12).[52] The deviation between the experimental and calculated absorption maxima in the low energy region were found to be in the range 435−740 cm^{-1}. One curious result, however, is the prediction that the HOMO predominantly resides on the pyrenyl-imidazole moiety in all the three cases. This finding contrasts with the electrochemical data, which clearly indicate that the first oxidation potential is not pyrenyl-imidazole-based and probably due to Ru^{II}/Ru^{III} oxidation process. However, it is not clear to us whether or not the HOMO mainly consisted of pyrenyl-imidazole moiety rather than the Ru(II) centers. In order to get a better understanding of the nature of the redox centers, we carried out DFT calculations on the two electron-oxidized forms of complexes **1** and **3**. The spin density plots of the oxidized forms of the complexes obtained from the optimized structures are shown in Figure 13, and the related Mulliken spin density distribution over different moieties is given in Table S5 (Supporting Information). On oxidation, the spin density is seen to be localized on the ruthenium center (0.884 for **1** and 0.838 for **3**) as well as on pyrenylimidazole moiety (0.910 for **1** and 0.888 for **3**). Thus, the spin density plots indicate that the ruthenium center is also actively involved in the oxidation process.

dx.doi.org/10.1021/ic501741r | Inorg. Chem. 2014, 53, 12036−12049

Triplet Excited-State and Calculated Luminescence Spectra. By performing UKS calculations on the triplet state, we were able to compute the energy difference between singlet and lowest energy triplet state of 1−3. The relevant results are shown in Tables S1, S2, and S4 and Figures S19 and S20 (Supporting Information). The geometries in the excited state resemble very closely those of the ground state. The calculated emission peak at 627, 635, and 645 nm was obtained for **1**, **2**, and **3**, respectively (Table S6, Supporting Information). As already discussed in the previous section, the experimental luminescence bands were obtained at 664, 670, and 703 nm for **1**, **2**, and **3**, respectively, in DMSO. It may be mentioned that the emission energy decreases, albeit to a small extent, as we go across the series from 1 to 3. Thus, the bathochromic shift of the experimental luminescence band on the variation of the terminal ligand from tpy to tpy-$PhCH_3$ and finally to H_2pbbzim is in line with the computed results.

CONCLUSION

In this Article we reported a joint experimental and computational study of three symmetrical rod-like bimetallic Ru(II) complexes derived from a bis-terpyridine bridging ligand containing pyrenyl-bis-phenylimidazole spacer. The photophysical and redox properties of the complexes were also fine-tuned by using three different terminal ligands with varying electronic properties. The attachment of pyrenyl-bis-phenylimidazole spacer to the $[Ru(tpy)_2]$ core was proven to be effective for the enhancement of light absorption properties of the complexes. The extensive delocalization of the charge-transfer excitation in these complexes also proves to be an effective way of tuning room-temperature luminescence properties of the complexes. Whereas the parent $[Ru(tpy)_2]^{2+}$ compound is essentially nonluminescent in fluid solution at room temperature, the newly synthesized bimetallic complexes exhibit room-temperature emission in the range of 657−703 nm with lifetimes between 5.8 and 67.0 ns, depending upon the terminal ligand as well as the solvent. Detailed temperature-dependent emission spectroscopic studies showed that decreasing temperature leads to an increase of emission intensity, quantum yield, and lifetime in all three cases. Thus, the favorable photophysical and electrochemical behaviors of these bimetallic Ru(II) complexes make them potential candidates as light-harvesting materials. Moreover, the electronic communication between the two ruthenium centers was evidenced by the presence of intervalence charge transfer transition (IVCT) bands in the NIR region of the spectrum when the mixed-valence species (Ru^{II}/Ru^{III}) are electrochemically generated. Analysis of the IVCT band indicates that this series of complexes exhibits relatively large couplings despite the large metal−metal distances (∼30 Å).

ASSOCIATED CONTENT

Supporting Information

$\{^1H-^1H\}$ COSY NMR, ESI mass, absorption, and luminescence spectra, and molecular orbital pictures related to DFT and TD-DFT calculation. This material is available free of charge via the Internet at http://pubs.acs.org

AUTHOR INFORMATION

Corresponding Author

*E-mail: sbaitalik@hotmail.com.

Notes

The authors declare no competing financial interest.

ACKNOWLEDGMENTS

The authors thank CSIR (India) as well as DST (India) for financial support through Grants 01(2766)/13/EMR-II and SR/S1/IC 33/2010 for this work. TCSPC facility under the DST-PURSE program of Department of Chemistry (JU) is also gratefully acknowledged. S.K. and D.M. acknowledge CSIR for their research fellowship. S.M. acknowledges UGC for his research fellowship.

REFERENCES

(1) Lewis, N. S.; Nocera, D. G. *Proc. Natl. Acad. Sci. U.S.A.* **2006**, *103*, 15729−15735.
(2) O'Regan, B.; Grätzel, M. *Nature* **1991**, *353*, 737−739.
(3) McNamara, W. R.; Snoeberger, R. C.; Li, G.; Schleicher, J. M.; Cady, C. W.; Poyatos, M.; Schmuttenmaer, C. A.; Crabtree, R. H.; Brudvig, G. W.; Batista, V. S. *J. Am. Chem. Soc.* **2008**, *130*, 14329−14338.
(4) Thompson, B. C.; Frechet, J. M. J. *Angew. Chem., Int. Ed.* **2008**, *120*, 62−82.
(5) (a) Du, P.; Schneider, J.; Jarosz, P.; Eisenberg, R. *J. Am. Chem. Soc.* **2006**, *128*, 7726−7727. (b) Chakraborty, S.; Wadas, T. J.; Hester, H.; Schmehl, R. H.; Eisenberg, R. *Inorg. Chem.* **2005**, *44*, 6865−6878.
(6) Gilat, S. L.; Adronov, A.; Fréchet, J. M. J. *Angew. Chem., Int. Ed.* **1999**, *38*, 1422−1427.
(7) Frischmann, P. D.; Mahata, K.; Würthner, F. *Chem. Soc. Rev.* **2013**, *42*, 1847−1870.
(8) Sautter, A.; Kaletas, B. K.; Schmid, D. G.; Dobrawa, R.; Zimine, M.; Jung, G.; van Stokkum, I. H. M.; De Cola, L.; Williams, R. M.; Würthner, F. *J. Am. Chem. Soc.* **2005**, *127*, 6719−6729.
(9) Fermi, A.; Ceroni, P.; Roy, M.; Gingras, M.; Bergamini, G. *Chem. Eur. J.* **2014**, *20*, 10661−10668.
(10) (a) Balzani, V.; Credi, A.; Venturi, M. *Molecular Devices and Machines*; Wiley-VCH: Weinheim, 2003. (b) Sun, L.; Hammarström, L.; Akermark, B.; Styring, S. *Chem. Soc. Rev.* **2001**, *30*, 36−49. (c) Wang, X.; Guerzo, A.; Baitalik, S.; Simon, G.; Shaw, G. B.; Chen, L. X.; Schmehl, R. *Photosynth. Res.* **2006**, *87*, 83−103. (d) Browne, W. R.; O'Boyle, N. M.; McGarvey, J. J.; Vos, J. G. *Chem. Soc. Rev.* **2005**, *34*, 641−663. (e) Balzani, V.; Clemente-Léon, M.; Credi, A.; Ferrer, B.; Venturi, M.; Flood, A. H.; Stoddart, J. F. *Proc. Natl. Acad. Sci. U.S.A.* **2006**, *103*, 1178−1183. (f) Manner, V. W.; DiPasquale, A. G.; Mayer, J. M. *J. Am. Chem. Soc.* **2008**, *130*, 7210−7211. (g) Manner, V. W.; Mayer, J. M. *J. Am. Chem. Soc.* **2009**, *131*, 9874−9875. (h) Miyazaki, S.; Kojima, T.; Mayer, J. M.; Fukuzumi, S. *J. Am. Chem. Soc.* **2009**, *131*, 11615−11624.
(11) De Silva, A. P.; Gunaratne, H. Q. N.; Gunnlaugsson, T.; Huxley, J. M.; McCoy, C. P.; Rademacher, J. T.; Rice, T. E. *Chem. Rev.* **1997**, *97*, 1515−1566.
(12) (a) Sauvage, J.-P.; Collin, J.-P.; Chambron, J.-C.; Guillerez, S.; Coudret, C.; Balzani, V.; Barigelletti, F.; De Cola, L.; Flamigni, L. *Chem. Rev.* **1994**, *94*, 993−1019. (b) McMillin, D. R.; Moore, J. J. *Coord. Chem. Rev.* **2002**, *229*, 113−121. (c) Hofmeier, H.; Schubert, U. S. *Chem. Soc. Rev.* **2004**, *33*, 373−399. (d) Wang, X.-Y.; Del Guerzo, A.; Schmehl, R. H. *J. Photochem. Photobiol., C* **2004**, *5*, 55−77. (e) Medlycott, E. A.; Hanan, G. S. *Chem. Soc. Rev.* **2005**, *34*, 133−146. (f) Medlycott, E. A.; Hanan, G. S. *Coord. Chem. Rev.* **2006**, *250*, 1763−1782. (g) Constable, E. C. *Chem. Soc. Rev.* **2007**, *36*, 246−253. (h) Pal, A. K.; Hanan, G. S. *Chem. Soc. Rev.* **2014**, *43*, 6184−6197.
(13) (a) Chakraborty, S.; Wadas, T. J.; Hester, H.; Flaschenreim, C.; Schmehl, R. H.; Eisenberg, R. *Inorg. Chem.* **2005**, *44*, 6284−6293. (b) Du, P.; Schneider, J.; Brennessel, W. W.; Eisenberg, R. *Inorg. Chem.* **2008**, *47*, 69−77. (c) Han, A.; Du, P.; Sun, Z.; Wu, H.; Jia, H.; Zhang, R.; Liang, Z.; Cao, R.; Eisenberg, R. *Inorg. Chem.* **2014**, *53*, 3338−3344.
(14) (a) Wild, A.; Friebe, C.; Winter, A.; Hager, M. D.; Grummt, U. W.; Schubert, U. S. *Eur. J. Org. Chem.* **2010**, 1859−1868. (b) Wild, A.; Schlütter, F.; Pavlov, G. M.; Friebe, C.; Festag, G.; Winter, A.; Hager, M. D.; Cimrová, V.; Schubert, U. S. *Macromol. Rapid Commun.* **2010**, *31*, 868−874. (c) Presselt, M.; Dietzek, B.; Schmitt, M.; Popp, J.;

Winter, A.; Chiper, M.; Friebe, C.; Schubert, U. S. *J. Phys. Chem. C* **2008**, *112*, 18651−18668. (d) Harriman, A.; Hissler, M.; Khatyr, A.; Ziessel, R. *Eur. J. Inorg. Chem.* **2003**, 955−959. (e) Fallahpour, R. A. *Synthesis* **2003**, 155. (f) Heller, M.; Shubert, U. S. *Synlett* **2002**, 751−754.
(15) Winkler, J. R.; Netzel, T. L.; Creutz, C.; Sutin, N. *J. Am. Chem. Soc.* **1987**, *109*, 2381−2392.
(16) (a) Coe, B. J.; Thompson, B. W.; Culbertson, C. D.; Shoonover, J. R.; Meyer, T. J. *Inorg. Chem.* **1995**, *34*, 3385−3395. (b) Kirchoff, J. R.; McMillin, D. R.; Marnot, P. A.; Sauvage, J.-P. *J. Am. Chem. Soc.* **1985**, *107*, 1138−1141.
(17) (a) Maestri, M.; Armaroli, N.; Balzani, V.; Constable, E. C.; Thompson, A. M. W. C. *Inorg. Chem.* **1995**, *34*, 2759−2767. (b) Wang, J.; Fang, Y. Q.; Hanan, G. S.; Loiseau, F.; Campagna, S. *Inorg. Chem.* **2005**, *44*, 5−7.
(18) (a) Fang, Y. Q.; Taylor, N. J.; Hanan, G. S.; Loiseau, F.; Passalacqua, R.; Campagna, S.; Nierengarten, H.; Van Dorsselaer, A. *J. Am. Chem. Soc.* **2002**, *124*, 7912−7913. (b) Passalacqua, R.; Loiseau, F.; Campagna, S.; Fang, Y. Q.; Hanan, G. S. *Angew. Chem., Int. Ed.* **2003**, *42*, 1608−1611. (c) Polson, M. I. J.; Loiseau, F.; Campagna, S.; Hanan, G. S. *Chem. Commun.* **2006**, 1301−1303. (d) Fang, Y. Q.; Taylor, N. J.; Laverdiere, F.; Hanan, G. S.; Loiseau, F.; Nastasi, F.; Campagna, S.; Nierengarten, H.; Leize-Wagner, E.; Van Dorsselaer, A. *Inorg. Chem.* **2007**, *46*, 2854−2863.
(19) (a) Hissler, M.; El-ghayoury, A.; Harriman, A.; Ziessel, R. *Angew. Chem., Int. Ed.* **1998**, *37*, 1717−1720. (b) Encinas, S.; Flamigni, L.; Barigelletti, F.; Constable, E. C.; Housecroft, C. E.; Schofield, E. R.; Figgemeier, E.; Fenske, D.; Neuburger, M.; Vos, J. G.; Zehnder, M. *Chem.—Eur. J.* **2002**, *8*, 137−150. (c) Benniston, A. C.; Harriman, A.; Li, P.; Sams, C. A. *J. Am. Chem. Soc.* **2005**, *127*, 2553−2664. (d) Wang, X-y.; Del Guerzo, A.; Tunuguntla, H.; Schmehl, R. H. *Res. Chem. Intermed.* **2007**, *33*, 63−77.
(20) (a) Duati, M.; Fanni, S.; Vos, J. G. *Inorg. Chem. Commun.* **2000**, *3*, 68−70. (b) Duati, M.; Tasca, S.; Lynch, F. C.; Bohlen, H.; Vos, J. G.; Stagni, S.; Ward, M. D. *Inorg. Chem.* **2003**, *42*, 8377−8384.
(21) (a) Constable, E. C.; Dunne, S. J.; Rees, D. G. F.; Schmitt, C. X. *Chem. Commun.* **1996**, 1169−1170. (b) Indelli, M. T.; Bignozzi, C. A.; Scandola, F.; Collin, J.-P. *Inorg. Chem.* **1998**, *37*, 6084−6089.
(22) (a) Beley, M.; Collin, J.-P.; Louis, R.; Metz, B.; Sauvage, J.-P. *J. Am. Chem. Soc.* **1991**, *113*, 8521−8522. (b) Wilkinson, A. J.; Puschmann, H.; Howard, J. A. K.; Foster, C. E.; Williams, J. A. G. *Inorg. Chem.* **2006**, *45*, 8685−8699. (c) Wadman, S. H.; Lutz, M.; Tooke, D. M.; Spek, A. L.; Hartl, F.; Havenith, R.W. A.; van Klink, G. P. M.; van Koten, G. *Inorg. Chem.* **2009**, *48*, 1887−1900.
(23) (a) Abrahamsson, M.; Jäger, M.; Österman, T.; Eriksson, L.; Persson, P.; Becker, H. C.; Johansson, O.; Hammarström, L. *J. Am. Chem. Soc.* **2006**, *128*, 12616−11617. (b) Abrahamsson, M.; Jäger, M.; Kumar, R. J.; Österman, T.; Persson, P.; Becker, H. C.; Johansson, O.; Hammarström, L. *J. Am. Chem. Soc.* **2008**, *130*, 15533−15542.
(24) (a) Bhaumik, C.; Das, S.; Saha, D.; Dutta, S.; Baitalik, S. *Inorg. Chem.* **2010**, *49*, 5049−5062. (b) Bhaumik, C.; Saha, D.; Das, S.; Baitalik, S. *Inorg. Chem.* **2011**, *50*, 12586−12600. (c) Bhaumik, C.; Das, S.; Maity, D.; Baitalik, S. *Dalton Trans.* **2012**, *41*, 2427−2438. (d) Maity, D.; Das, S.; Mardanya, S.; Baitalik, S. *Inorg. Chem.* **2013**, *52*, 6820−6838.
(25) (a) Breivogel, A.; Förster, C.; Heinze, K. *Inorg. Chem.* **2010**, *49*, 7052−7056. (b) Dietrich, J.; von Leupoldt, A. W.; Grabolle, M.; Resch-Genger, U.; Heinze, K. *Eur. J. Inorg. Chem.* **2013**, 3009−3019. (c) Breivogel, A.; Hempel, K.; Heinze, K. *Inorg. Chim. Acta* **2011**, *374*, 152−162.
(26) McClenaghan, N. D.; Leydet, Y.; Maubert, B.; Indelli, M. T.; Campagna, S. *Coord. Chem. Rev.* **2005**, *249*, 1336−1350.
(27) (a) Wrighton, M. S.; Morse, D. L.; Pdungsap, L. *J. Am. Chem. Soc.* **1975**, *97*, 2073−2079. (b) Fredericks, S. M.; Luong, J. C.; Wrighton, M. S. *J. Am. Chem. Soc.* **1979**, *101*, 7415−7417.
(28) Ford, W. E.; Rodgers, M. A. J. *J. Phys. Chem.* **1992**, *96*, 2917−2920.
(29) Wilson, G. J.; Launikonis, A.; Sasse, W. H. F.; Mau, A. W. H. *J. Phys. Chem. A* **1997**, *101*, 4860−4866.
(30) (a) Grusenmeyer, T. A.; Chen, J.; Jin, Y.; Nguyen, J.; Rack, J. J.; Schmehl, R. H. *J. Am. Chem. Soc.* **2012**, *134*, 7497−7506. (b) Gu, J.; Chen, J.; Schmehl, R. H. *J. Am. Chem. Soc.* **2010**, *132*, 7338−7346. (c) Simon, J. A.; Curry, S. L.; Schmehl, R. H.; Schatz, T. R.; Piotrowiak, P.; Jin, X.; Thummel, R. P. *J. Am. Chem. Soc.* **1997**, *119*, 11012−11022. (d) Balazs, G. C.; del Guerzo, A.; Schmehl, R. H. *Photochem. Photobiol. Sci.* **2005**, *4*, 89−94. (e) Del Guerzo, A.; Leroy, S.; Fages, F.; Schmehl, R. H. *Inorg. Chem.* **2002**, *41*, 359−366.
(31) (a) Tyson, D. S.; Castellano, F. N. *J. Phys. Chem. A* **1999**, *103*, 10955−10960. (b) Tyson, D. S.; Luman, C. R.; Zhou, X.; Castellano, F. N. *Inorg. Chem.* **2001**, *40*, 4063−4071. (c) Kozlov, D. V.; Tyson, D. S.; Goze, C.; Ziessel, R.; Castellano, F. N. *Inorg. Chem.* **2004**, *43*, 6083−6092.
(32) Sohna Sohna, J.; Carrier, V.; Fages, F.; Amouyal, E. *Inorg. Chem.* **2001**, *40*, 6061−6063.
(33) Ji, S.; Wu, W.; Wu, W.; Guo, H.; Zhao, J. *Angew. Chem., Int. Ed.* **2011**, *50*, 1626−1629.
(34) (a) Morales, A. F.; Accorsi, G.; Armaroli, N.; Barigelletti, F.; Pope, S. J. A.; Ward, M. D. *Inorg. Chem.* **2002**, *41*, 6711−6719. (b) Maubert, B.; McClenaghan, N. D.; Indelli, M. T.; Campagna, S. *J. Phys. Chem. A* **2003**, *107*, 447−455. (c) McClenaghan, N. D.; Barigelletti, F.; Maubert, B.; Campagna, S. *Chem. Commun.* **2002**, *6*, 602−603.
(35) (a) Harriman, A.; Hissler, M.; Khatyr, A.; Ziessel, R. *Chem. Commun.* **1999**, 735−736. (b) Hissler, M.; Harriman, A.; Khatyr, A.; Ziessel, R. *Chem.—Eur. J.* **1999**, *5*, 3366−3381. (c) Benniston, A. C.; Harriman, A.; Lawrie, D. J.; Mayeux, A. *Phys. Chem. Chem. Phys.* **2004**, *6*, 51−57.
(36) Michalec, J. F.; Bejune, S. A.; McMillin, D. R. *Inorg. Chem.* **2000**, *39*, 2708−2709.
(37) Maity, D.; Bhaumik, C.; Mondal, D.; Baitalik, S. *Inorg. Chem.* **2013**, *52*, 13941−13955.
(38) Demadis, K. D.; Hartshorn, C. M.; Meyer, T. J. *Chem. Rev.* **2001**, *101*, 2655−2686.
(39) Brunschwig, B. S.; Creutz, C.; Sutin, N. *Chem. Soc. Rev.* **2002**, *31*, 168−184.
(40) D'Alessandro, D. M.; Keene, R. F. *Chem. Soc. Rev.* **2006**, *35*, 424−440.
(41) Kaim, W.; Lahiri, G. K. *Angew. Chem., Int. Ed.* **2007**, *46*, 1778−1796.
(42) Hu, J.; Zhang, D.; Harris, F. W. *J. Org. Chem.* **2005**, *70*, 707−708.
(43) Krohnke, F. *Synthesis* **1976**, 1−24.
(44) (a) Xiaoming, X.; Haga, M.; Matsumura-Inoue, T.; Ru, Y.; Addison, A. W.; Kano, K. *J. Chem. Soc., Dalton Trans.* **1993**, 2477−2484. (b) Haga, M.; Takasugi, T.; Tomie, A.; Ishizuya, M.; Yamada, T.; Hossain, M. D.; Inoue, M. *Dalton Trans.* **2003**, 2069−2079.
(45) Juris, A.; Balzani, V.; Barigelletti, F.; Campagna, S.; Belser, P.; von Zelewsky, A. *Coord. Chem. Rev.* **1988**, *84*, 85−277.
(46) Rillema, D. P.; Blanton, C. B.; Shaver, R. J.; Jackman, D. C.; Boldaji, M.; Bundy, S.; Worl, L. A.; Meyer, T. J. *Inorg. Chem.* **1992**, *31*, 1600−1606.
(47) (a) Hush, N. S. *Prog. Inorg. Chem.* **1967**, *8*, 391−444. (b) Hush, N. S. *Electrochim. Acta* **1968**, *13*, 1005−1023. (c) Hush, N. S. *Coord. Chem. Rev.* **1985**, *64*, 135−167.
(48) (a) Oh, D. H.; Sano, M.; Boxer, S. C. *J. Am. Chem. Soc.* **1991**, *113*, 6880−6890. (b) Silverman, L. N.; Kanchanawomg, P.; Treynor, T. P.; Boxer, S. G. *Philos. Trans. R. Soc., A* **2008**, *366*, 33−45.
(49) Robin, M. B.; Day, P. *Adv. Inorg. Chem. Radiochem.* **1968**, *10*, 247−422.
(50) (a) Patoux, C.; Launay, J.-P.; Beley, M.; Chodorowski-Kimmes, S.; Collin, J.-P.; James, S.; Sauvage, J.-P. *J. Am. Chem. Soc.* **1998**, *120*, 3717−3725. (b) Fraysse, S.; Coudret, C.; Launay, J.-P. *J. Am. Chem. Soc.* **2003**, *125*, 5880−5888.
(51) (a) Chanda, N.; Sarkar, B.; Fiedler, J.; Kaim, W.; Lahiri, G. K. *Inorg. Chem.* **2004**, *43*, 5128−5133. (b) Ghumann, S.; Sarkar, B.; Chanda, N.; Sieger, M.; Fiedler, J.; Kaim, W.; Lahiri, G. K. *Inorg. Chem.* **2006**, *45*, 7955−7961.

(52) (a) Sinn, S.; Schulze, B.; Friebe, C.; Brown, D. G.; Jäger, M.; Kübel, J.; Dietzek, B.; Berlinguette, C. P.; Schubert, U. S. *Inorg. Chem.* **2014**, *53*, 1637−1645. (b) Sinn, S.; Schulze, B.; Friebe, C.; Brown, D. G.; Jäger, M.; Altuntas, E.; Kübel, J.; Gunter, O.; Berlinguette, C. P.; Dietzek, B.; Schubert, U. S. *Inorg. Chem.* **2014**, *53*, 2083−2095. (c) Wächtler, M.; Kupfer, S.; Guthmuller, J.; Popp, J.; González, L.; Dietzek, B. *J. Phys. Chem. C* **2011**, *115*, 24004−24012. (d) Wächtler, M.; Kupfer, S.; Guthmuller, J.; Rau, S.; González, L.; Dietzek, B. *J. Phys. Chem. C* **2012**, *116*, 25664−25676.